

Article

## Gas Atomization of Aluminium Melts: Comparison of Analytical Models

Georgios Antipas

School of Mining Engineering and Metallurgy, National Technical University of Athens, Zografou Campus, Athens 15780, Greece; E-Mail: gantipas@metal.ntua.gr; Tel.: +30-210-772-2388

Received: 31 March 2012; in revised form: 28 May 2012 / Accepted: 6 June 2012 /

Published: 18 June 2012

---

**Abstract:** A number of analytical models predicting the size distribution of particles during atomization of Al-based alloys by N<sub>2</sub>, He and Ar gases were compared. Simulations of liquid break up in a close coupled atomizer revealed that the finer particles are located near the center of the spray cone. Increasing gas injection pressures led to an overall reduction of particle diameters and caused a migration of the larger powder particles towards the outer boundary of the flow. At sufficiently high gas pressures the spray became monodisperse. The models also indicated that there is a minimum achievable mean diameter for any melt/gas system.

**Keywords:** Al alloys; gas atomization; spray forming; two phase flow; liquid break up; surface wave formation

---

### 1. Introduction

In metal spray forming, the atomization parameters define the size of the powders to be deposited on the substrate. The size of the particles and their position inside the spray affect their cooling histories and the solid fraction on the preform. The quality of the end product depends very much on porosity, grain size and distribution of intermetallic phases in the powder, all of which are in turn a function of the cooling histories of the powder particles in flight. It, therefore, follows that information on the dynamic behaviour of the drops is needed for an accurate prediction of the shape and quality of the preform or the mean diameter and the microstructure of the powder collected. A first major step in this direction is the prediction of the liquid break up mechanisms during gas atomization.

In gas atomization a liquid metal stream is perturbed by a number of high velocity gas jets and is broken up into fine drops [1] which solidify in flight. In the first stage, that of primary atomization, the

surface of the melt is disturbed by a sinusoidal oscillation [2] and is subsequently broken up into large drops or unstable bodies, the ligaments [3]. During the subsequent stage of secondary atomization, the drops/ligaments may further disintegrate in flight, either via a low-turbulence mechanism [4] or in a more chaotic high-turbulence stripping fashion [5]. Gas flow characteristics at the point of atomization as well as further downstream affect the modes of metal break up and consequently determine the size and mass distribution of the resulting spray. Drop size and mass distribution, two-phase turbulence effects and heat transfer during solidification in turn determine the metallurgical quality of the preform. Atomization process control has been considered in earlier phenomenological studies [6–14] in respect to atomization parameters—such as nature of the gas and melt phase, gas injection pressures and melt superheat. More recently, experimental treatises of atomizing geometries have been presented [15–17]. Solidification modeling and process control frequently rely on powder size calculated from empirical equations, e.g., the Lubanska equation [18]. However, such empirical equations do not yield drop size or mass distributions inside the spray cone. Liquid break up phenomena, in turn—although described in the macro scale early on [19–22]—have not been reflected on rigorous modelling implementations. Modern atomization modeling appears to be focusing on CPU-intensive stochastic simulation of the liquid jet and primary atomization in terms of Reynolds-averaged Navier-Stokes mixing [23]. Recently, the more realistic cases of turbulent atomization conditions have been addressed, e.g., by computational fluid dynamics (CFD) [24–26] and integrated models [17,27] have been proposed.

This study presents a comparison of principal analytical models used in engineering practice, addressing primary and secondary break up. The models have been applied to the atomization of Al melts. In a previous study of He atomized Al alloys [28] the mean powder size appeared largely uninfluenced by secondary alloying elements, effectively behaving as bulk Al. Accordingly, the current study considers Al as the melt phase and results of the radial distribution of powder sizes are presented for a variety of atomization conditions, in a close coupled atomizer assembly. Particulars of the atomizer geometry, generated gas flow as well as the transport equations used for the particles in flight have been described in [29].

## 2. Break Up Models

The first algorithm considered is based on the Surface Wave Formation (SWF model) theory and has been explained in [30]; the key concepts of the model are reproduced here for the sake of completeness. In the SWF model of primary break up, a single, fastest growing wavelength, induced by the sonic velocity of the atomizer gas jets, is taken to be responsible for the primary deformation of the melt stream. The wave has a phase (propagation) velocity downstream which in turn creates crests and troughs along the liquid column; when the crests reach a critical height, an unstable ligament is assumed to be formed via stripping of a part of the crest, or detached from the liquid column at points of negative amplitude. The critical height,  $n_c$ , is defined as:

$$n_c = \frac{2\sigma}{\frac{1}{2}C_D\rho_g U_r^2} \quad (1)$$

where  $\sigma$  is the liquid surface tension;  $C_D$  is the drag coefficient;  $\rho_g$  is the gas density and  $U_r$  is the relative velocity between the liquid and the gas phase. The SWF model utilizes a force balance criterion to calculate the critical amplitude for specific gas and metal properties above which stripping of the tip of the crest or detachment of the liquid column occurs. In this way, the fastest growing wavelength is related to a critical amplitude and for every crest with an amplitude exceeding the critical one, the diameter and volume of the ring-shaped ligament are also determined. The SWF model of secondary break up—*i.e.*, disintegration of a ligament or drop into smaller fragments—assumes a cylindrical liquid shape perturbed by a wide array of wavelengths (and their corresponding growth rates) and is transported inside the flow in a lagrangian fashion, governed by the equation:

$$m_p \frac{dU_p}{dt} = \frac{1}{2} C_D \rho_g U_r^2 A + m_p g \quad (2)$$

where  $m_p$  is the mass of the particle being transported,  $U_p$  is the velocity of the particle,  $A$  is the area of the particle seen by the gas flow and  $g$  is the gravitational acceleration.

The second model is based on a drop break up criterion, termed the Weber model, which is based on observations made by Hinze [31]. According to this, for a given set of liquid drop and gas properties, there is a critical stable size,  $D_c$ , above which the drop will break into smaller fragments. This critical size is related to the critical Weber number,  $(N_{we})_c$ , through the expression:

$$D_c = \frac{(N_{we})_c \sigma}{\rho_g U_r^2} \quad (3)$$

Any drop exceeding the critical size is instantaneously broken into fragments of the critical diameter. The number of fragments is equal the ratio of mass of the initial drop to that of the critical size. In practise, the actual value of the critical Weber number first needs to be evaluated for a particular melt/gas system and for a given set of injection parameters by trial and error. Afterwards, that critical value can be used for any other set of conditions for that particular system.

An analytical model for drop break up originally presented by Wolf and Andersen [32] and revised in the current work to take into account the effect of the drag coefficient, was also put under scrutiny (WA model). In the original WA approach, a drop of cylindrical shape of length  $l_c$  is assumed. The gas pressures necessary to cause either a hollow bag or a stripping break up were calculated. The pressure for the hollow bag mechanism,  $P_b$ , is given by Equation (4), while the pressure necessary for the stripping mode,  $P_s$ , is given by Equation (5):

$$P_b = \frac{1}{3} \frac{C_D \rho_g U_r^2}{2} - \frac{\sigma}{D_c} \quad (4)$$

$$P_s = \frac{2}{3} \frac{C_D \rho_g U_r^2}{2} - \frac{4\sigma}{D_c} \quad (5)$$

The pressure that is positive and larger between Equations (4) and (5) was selected to be the driving force of the disintegration. The displacement of an assumed outer layer of the drop in respect to the undisturbed position of its free surface was then calculated. If at any time the displacement was found to be equal or larger than the diameter of the initial drop, the outer layer was broken into fragments with dimensions,  $y$ ,  $L$  and  $W$ , given by Equations (6), (7) and (8), respectively:

$$y = \frac{4 \mu_l}{U_r \sqrt{\rho_g \rho_l}} \quad (6)$$

$$L = \frac{4 \pi \sigma}{\rho_g U_r^2} \quad (7)$$

$$W = \frac{l_c}{2 U_r} \sqrt{\frac{8 \sigma}{l_c C_D \rho_g}} \quad (8)$$

where  $\mu_l$  is the dynamic viscosity of the melt; for liquid Al,  $\mu_l$  is taken to be 1.0 mPa·s. The diameter of each drop,  $D_s$ , produced in this manner is given by the expression:

$$D_s = \sqrt[3]{\frac{6}{\pi} y L W} \quad (9)$$

and the number,  $N_s$ , of drops produced was expressed as:

$$N_s = \frac{\pi D_o y L}{W y L} = \frac{\pi D_o}{W} \quad (10)$$

by dividing the volume of the stripped layer by the volume of the assumed drops formed by its collapse.

Finally, the empirical Lubanska equation [18] was employed to correlate the mass median diameter,  $D_m$ , to the processing parameters of atomization:

$$D_m = D_o C_L \left[ \frac{\nu}{\nu_g N_{We}} \right]^{1/2} \quad (11)$$

where  $C_L$  is a numerical constant ranging from 40 to 50;  $\nu_l$  and  $\nu_g$  are the liquid and gas kinematic viscosities; respectively,  $D_o$  is the initial diameter of the melt and  $N_{We}$  is the Weber number defined as:

$$N_{We} = \frac{\rho_g U_r^2 D_o}{\sigma} \quad (12)$$

In the current study, the kinematic viscosity of liquid Al at 1100 °C was taken to be  $3.10 \times 10^{-7}$  m<sup>2</sup>/s, while the kinematic viscosities of N<sub>2</sub>, He and Ar at 20 °C were  $1.51 \times 10^{-5}$ ,  $1.17 \times 10^{-4}$  and  $1.34 \times 10^{-5}$  m<sup>2</sup>/s, respectively.

Primary atomization, *i.e.*, the breakdown of a liquid column into spherical drops was always calculated by the SWF model. The particles created during primary atomization were then used as input data for the models mentioned above. Unless otherwise stated, the atomization parameters were kept constant throughout the simulations and are as follows:

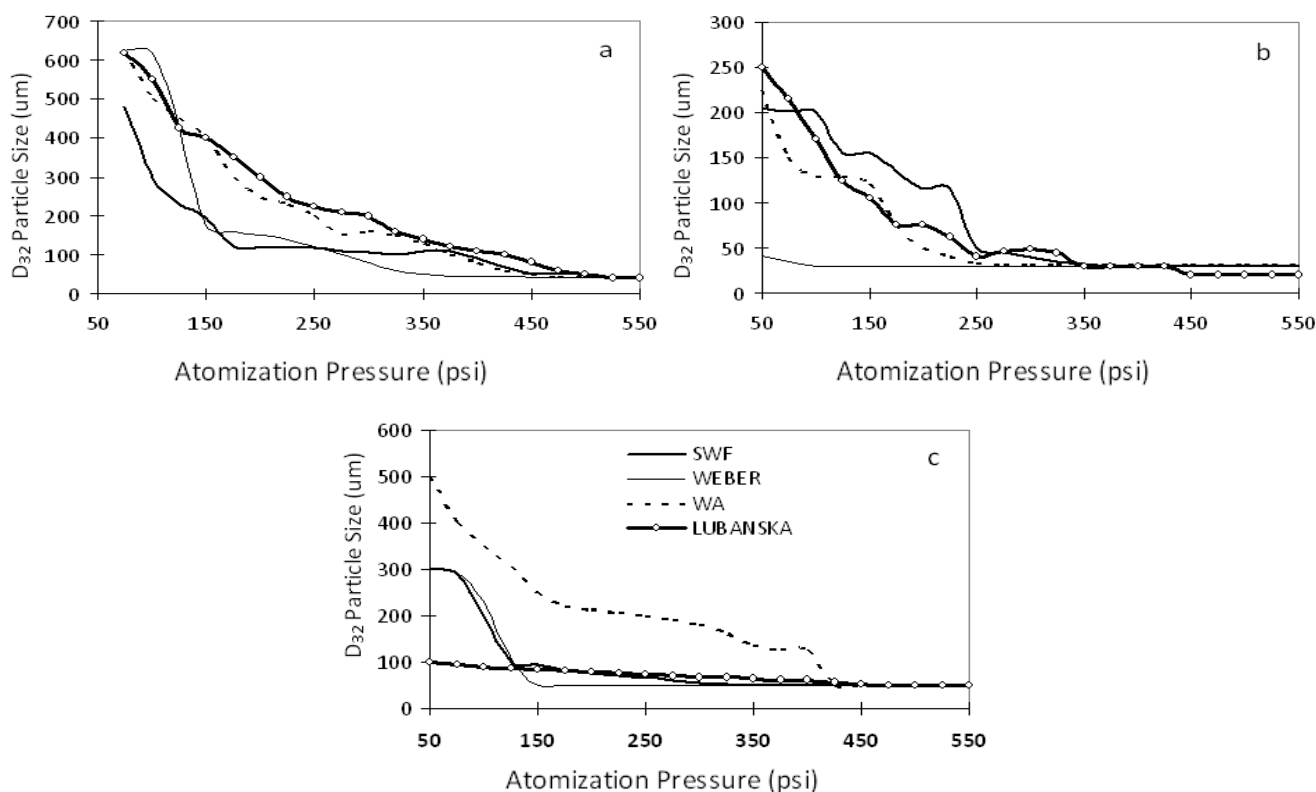
1. Atomization Pressure : 150 psi (1.03 MPa);
2. Ambient Pressure : 14 psi (0.096 MPa);
3. Initial Melt Column Radius : 0.001 m;
4. Initial Melt Exit Velocity : 1 m/s;
5. End of break up calculations 0.4 m downstream of atomizer.

### 3. Results and Discussion

The behavior of the atomization models was studied as a function of the injection pressure and type of gas. The parameter considered was the Sauter  $D_{32}$  particle size for which the overall and localized-radial values were calculated.

Figure 1(a–c) illustrate the effect of increasing injection pressure for  $N_2$ , He and Ar, respectively, on the overall  $D_{32}$  size for liquid Al. The Lubanska equation predicts finer particles for Ar than for He up to a pressure of 150 psi, above which the trend is reversed, in par with experimental evidence for the two gases [2]. A uniform trend shown by the SWF, Weber and WA models is the reduction of the  $D_{32}$  size with increasing pressure. In addition the models predict that He produces the finest powders under any atomization pressures. In addition,  $N_2$  yields coarser particles compared to Ar. The Weber model is not sensitive to the changes in the injection pressure of He.

**Figure 1.** Effect of the type of atomizing gas on the overall  $D_{32}$  particle size for Al (a)  $N_2$ ; (b) He; (c) Ar.



The radial distribution of particle sizes is shown in Figure 2(a–c) for  $N_2$ , Figure 3(a–d) for He and Figure 4(a–d) for Ar. At relatively low pressures, e.g., 50 psi (0.34 MPa), the particle size profiles for the different gases are non-uniform. At higher pressures, 100 psi (0.69 MPa), the profiles begin to follow the distinct pattern of finer particles in the center and coarser fragments in the outer regions of the flow. All models predict finer particles for He. Figure 2b, Figure 3c and Figure 4c show the trend of the flow towards a monodisperse array of drops radially, with the largest of particles being pushed towards the edge of the spray.

**Figure 2.** Predicted radial variation of the  $D_{32}$  size for Al-N<sub>2</sub> at (a) 100 psi (0.69 mpa); (b) 200 psi (1.38 mpa); (c) 300 psi (2.07 MPa).

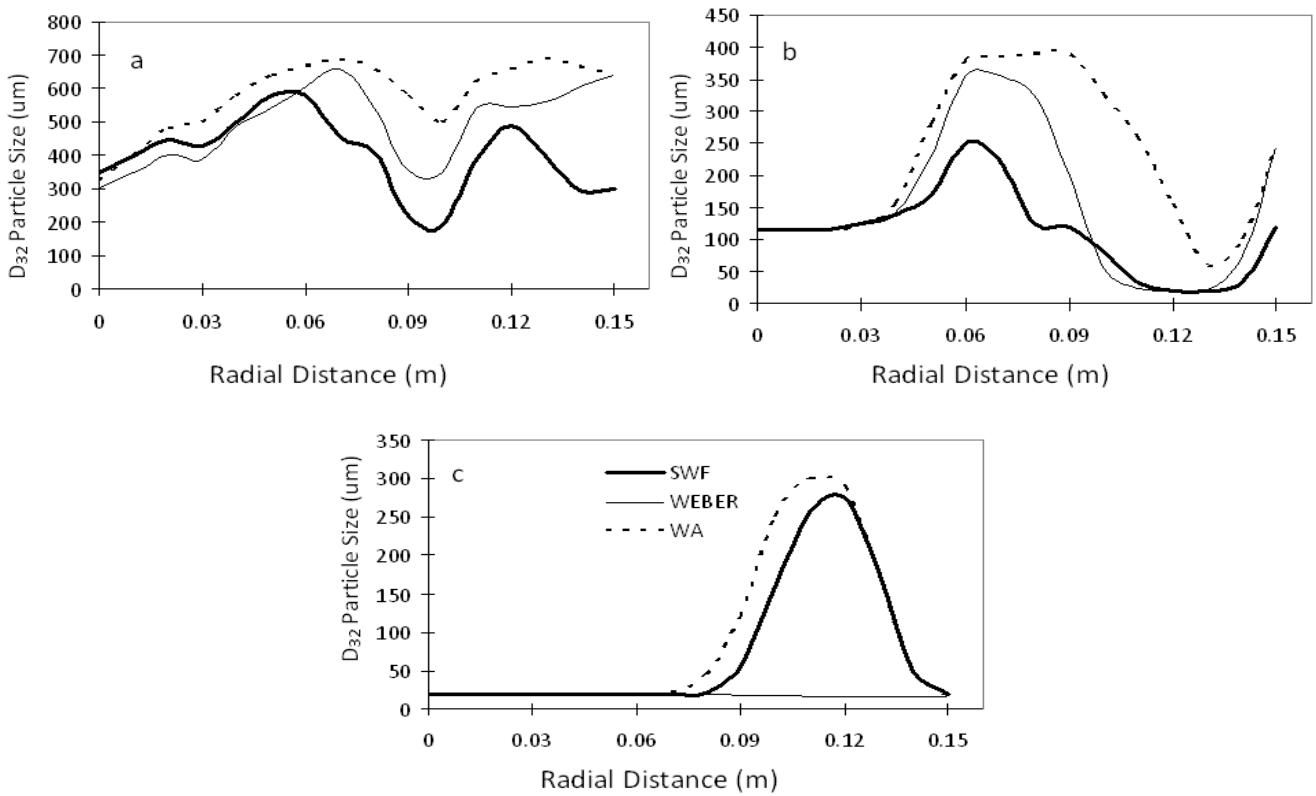


**Figure 3.** Predicted radial variation of the  $D_{32}$  size for Al-He at (a) 50 psi (0.34 mpa); (b) 100 psi (0.69 MPa); (c) 200 psi (1.38 mpa); (d) 300 psi (2.07 MPa).

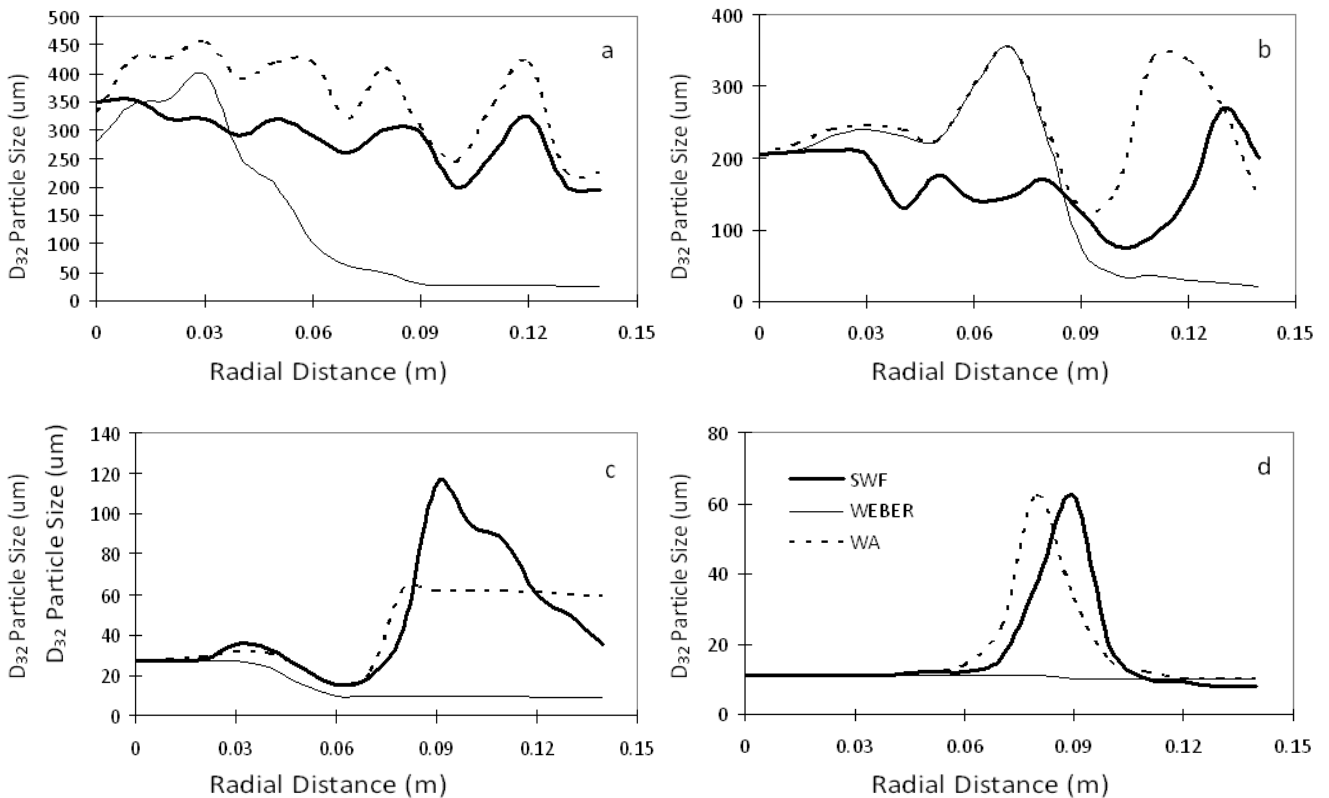
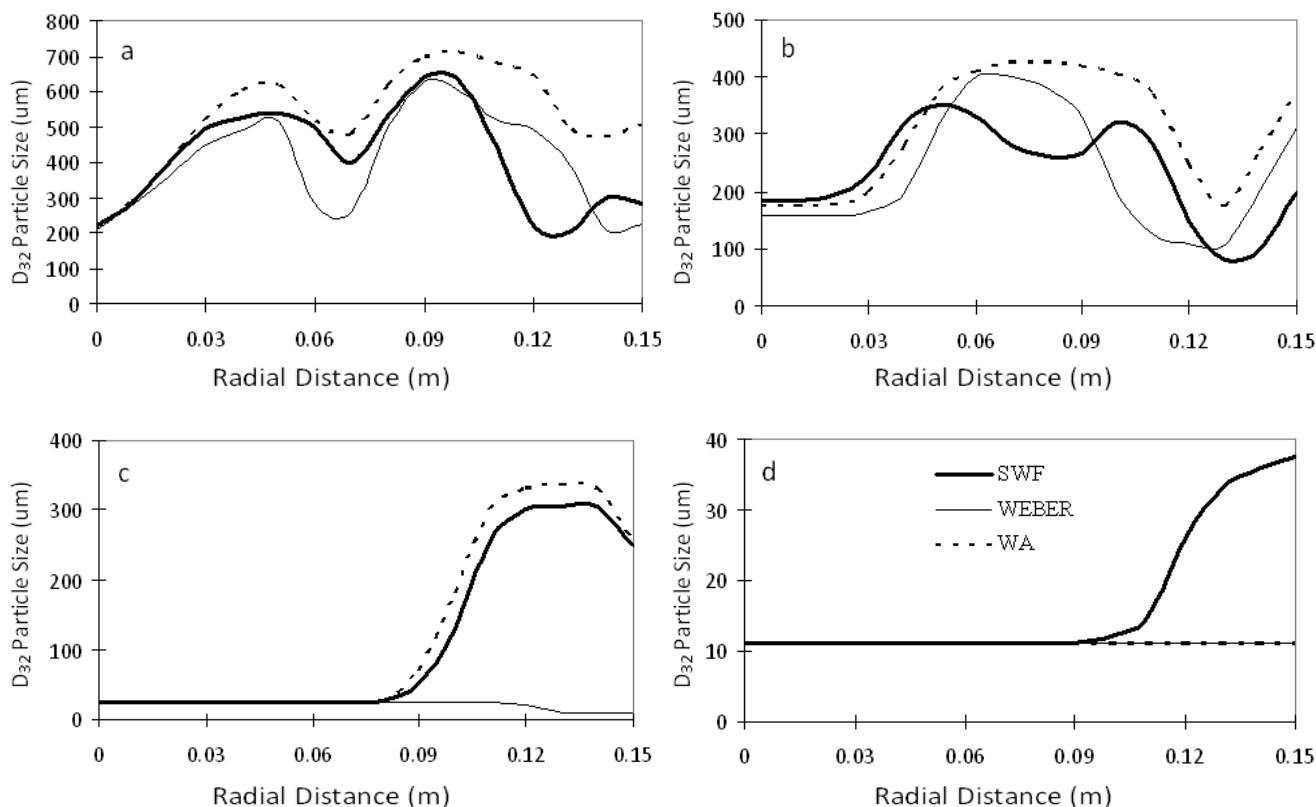


**Figure 4.** Predicted radial variation of the  $D_{32}$  size for Al-Ar at (a) 50 psi (0.34 mpa); (b) 100 psi (0.69 MPa); (c) 200 psi (1.38 mpa); (d) 300 psi (2.07 mpa).



Increasing gas pressure with a fixed initial melt velocity amounts to an increasing gas to melt mass flux ratio, and as expected the Lubanska expression predicts a continuous decrease in drop sizes as do the three break up models, e.g., see Figure 1(a–c). An important feature of the plot is the region of high pressures (300 psi–2.07 MPa and over) where the rate of decrease for the particle size remains roughly constant. This indicates that after a certain threshold is exceeded for the gas pressure, any surplus in energy offered to the melt will not contribute to further break up.

The effect of the gas pressure on the  $D_{32}$  size can be understood by inspection of Figure 3(a–d) as an example. At low pressures, e.g., Figure 3a, the fragmentation of the large globules formed during primary break up is incomplete. The two easily distinguishable crests 5 cm and 10 cm away from the central axis are in fact regions of large primary globules having undergone break up. As the atomization pressure becomes higher, Figure 3b, there is a noticeable decrease in the larger fragments of the spray, while the finer ones are unaffected. This indicates that splitting of a large particle is easier in comparison to a smaller one for the same set of conditions, which in fact is the basis of the Weber model. A further increase in gas pressures causes a shift of the coarse particles towards the outer regions of the spray, as shown in Figure 3c. The fine fragments in this case cover a considerable radial spread, as predicted by SWF and WA, while the Weber model indicates uniformity along the radial direction. Figure 3d shows a further reduction of sizes, but the radial gradient in sizes still exists, as predicted by SWF, while WA and Weber predict complete break up. The spray is now dominated by fine particles of a uniform size, while the coarse fragments have been pushed further away from the center. The size gap between fine and coarse particles is reduced.

#### 4. Conclusions

The predicted break up events in two phase flows by the SWF, Weber and WA models, revealed that the radial distribution of particle sizes was that fine particles existed near the center axis and coarser ones with increasing distance from the center. At sufficiently high injection pressures a monodisperse spray of fine powders was produced, with the coarse particles being pushed to the outer edge of the flow. At very high gas pressures, break up reached a saturation point in the center of the flow and there was no detectable radial gradient of particle sizes. Helium was found to produce the finest particles under any set of atomization conditions with nitrogen producing the coarsest ones. Due to its inherent affinity with Kelvin-Helmholtz theory, the SWF model offers enhanced insight regarding the radial distribution of particle sizes, which the rest of the models lack. The WA model offers some accountability towards radial distribution of sizes but due to the deterministic nature of the twin break up mechanism on which it operates, it has a bias towards monodisperse particle distributions.

#### References

1. Dumouchel, C.; Cousin, J.; Triballier, K. Experimental analysis of liquid-gas interface at low weber number: Interface length and fractal dimension. *Exp. Fluids* **2005**, *39*, 651–666.
2. Fei, L.S.; Xu, S.L.; Wang, C.J.; Li, Q.; Huang, S.H. Experimental study on atomization phenomena of kerosene in supersonic cold flow. *Sci. China E Technol. Sci.* **2008**, *51*, 145–152.
3. Shinjo, J.; Umemura, A. Simulation of liquid jet primary breakup: Dynamics of ligament and droplet formation. *Int. J. Multiph. Flow* **2010**, *36*, 513–532.
4. Ng, C.L.; Sankar Krishnana, R.; Sallam, K.A. Bag breakup of nonturbulent liquid jets in crossflow. *Int. J. Multiph. Flow* **2008**, *34*, 241–259.
5. Guildenbecher, D.R.; López-Rivera, C.; Sojka, P.E. Secondary atomization. *Exp. Fluids* **2009**, *46*, 371–402.
6. See, J.; Johnston, G. Interactions between nitrogen jets and liquid lead and tin streams. *Powder Technol.* **1978**, *21*, 119–133.
7. Kim, M.; Jones, H. Effect of process variables in gas-jet atomization and production of multilayer deposits. In *Proceedings of the 4th International Conference on Rapidly Quenched Metal*, Sendi, Japan, 22–24 August 1988.
8. Hiroyasu, H.; Shimizu, M.; Arai, M. The breakup of a high speed jet in a high pressure gaseous atmosphere. In *Proceedings of the 2nd International Conference on Liquid Atomization and Spray Systems*, Madison, WI, USA, 20–24 June 1982.
9. Pai, B.; Nijaguna, B. The characterization of sprays. In *Proceedings of the 2nd International Conference on Liquid Atomization and Spray Systems*, Madison, WI, USA, 20–24 June 1982.
10. Reitz, R. Modelling atomization processes in high-pressure vaporizing sprays. *At. Spray Technol.* **1987**, *3*, 309–337.
11. Arai, M.; Shimizu, M.; Hiroyasu, H. Break-up length and spray formation mechanism of a high speed liquid jet. In *Proceedings of the 4th International Conference on Liquid Atomization and Spray Systems*, Sendai, Japan, 22–24 August 1988.
12. Ünal, A. Effect of processing variables on particle size in gas atomization of rapidly solidified aluminium powders. *Mater. Sci. Technol.* **1987**, *3*, 1029–1039.

13. Ingebo, R. Experimental and theoretical effects of nitrogen gas flow rate on liquid jet atomization. *J. Propuls. Power* **1988**, *4*, 406–411.
14. Zanelli, S. Behaviour of a liquid jet near the nozzle. In *Proceedings of the 4th International Conference on Liquid Atomization and Spray Systems*, Sendai, Japan, 22–24 August 1988.
15. Vahedi, T.H.; Pourdeyhimi, B. The effects of nozzle geometry on water jet breakup at high Reynolds numbers. *Exp. Fluids* **2003**, *35*, 364–371.
16. Vukasinovic, B.; Smith, M.K.; Glezer, A. Mechanisms of free-surface breakup in vibration-induced liquid atomization. *Phys. Fluids* **2007**, *19*, 012104:1–012104:15.
17. Dumouchel, C. On the experimental investigation on primary atomization of liquid streams. *Exp. Fluids* **2008**, *45*, 371–422.
18. Lubanska, H. Correction of spray ring data for gas atomization of liquid metals February. *J. Metals* **1970**, *22*, 45–49.
19. Hinze, J. Fundamentals of the hydrodynamic mechanism of splitting in dispersion processes. *AICHE J.* **1955**, *1*, 289–295.
20. Gordon, G. Mechanism and speed of breakup of drops. *J. App. Phys.* **1959**, *30*, 1759–1761.
21. Mehrota, S. Mathematical modelling of gas atomization process for metal powder production. *Powder Metall. Int.* **1988**, *13*, 80–84.
22. Haas, F. Stability of droplets suddenly exposed to a high velocity gas stream. *AICHE J.* **1964**, *10*, 920–924.
23. Gorokhovski, M.; Herrmann, M. Modeling primary atomization. *Annu. Rev. Fluid Mech.* **2008**, *40*, 343–366.
24. Ishimoto, J.; Ohira, K.; Okabayashi, K.; Chitose, K. Integrated numerical prediction of atomization process of liquid hydrogen jet. *Cryogenics* **2008**, *48*, 238–247.
25. Trinh, H.P.; Chen, C.P.; Balasubramanyam, M.S. Numerical simulation of liquid jet atomization including turbulence effects. *J. Eng. Gas Turb. Power* **2007**, *129*, 920–928.
26. Pougatcha, K.; Salcudeana, M.; Chanb, E.; Knapper, B. A two-fluid model of gas-assisted atomization including flow through the nozzle, phase inversion, and spray dispersion. *Int. J. Multiph. Flow* **2009**, *35*, 661–675.
27. Kumar, A.; Ghosh, S.; Dhindaw, B.K. Simulation of cooling of liquid Al-33 wt.% Cu droplet impinging on a metallic substrate and its experimental validation. *Acta Mater.* **2010**, *58*, 122–133.
28. Antipas, G.S.E. Spray forming of Al alloys: Experiment and theory. *Mater. Res.* **2012**, *15*, 131–135.
29. Antipas, G.S.E. Modelling of the break up mechanism in gas atomization of liquid metals, Part II. The gas flow model. *Comput. Mater. Sci.* **2009**, *46*, 955–959.
30. Antipas, G.S.E. Modelling of the break up mechanism in gas atomization of liquid metals, Part I. The surface wave formation model. *Comput. Mater. Sci.* **2006**, *35*, 416–422.
31. Hinze, J.O. Fundamentals of the hydrodynamic mechanism of splitting in dispersion process. *AICHE J.* **1955**, *1*, 289–295.
32. Wolf, H.E.; Andersen, W.H. Aerodynamic break-up of liquid drops. In *Proceedings of the 5th International Shock Tube Symposium*, Berkely, CA, USA, 28–30 April 1965.